Neuron modeling: estimating the parameters of a neuron model from neural spiking data

Reşat Özgür DORUK*

Department of Electrical and Electronics Engineering, Faculty of Engineering, Atılım University, Ankara, Turkey

Abstract: We present a modeling study aiming at the estimation of the parameters of a single neuron model from neural spiking data. The model receives a stimulus as input and provides the firing rate of the neuron as output. The neural spiking data will be obtained from point process simulation. The resultant data will be used in parameter estimation based on the inhomogeneous Poisson maximum likelihood method. The model will be stimulated by various forms of stimuli, which are modeled by a Fourier series (FS), exponential functions, and radial basis functions (RBFs). Tabulated results presenting cases with different sample sizes (# of repeated trials), stimulus component sizes (FS and RBF), amplitudes, and frequency ranges (FS) will be presented to validate the approach and provide a means of comparison. The results showed that regardless of the stimulus type, the most effective parameter on the estimation performance appears to be the sample size. In addition, the lowest variance of the estimates is obtained when a Fourier series stimulus is applied in the estimation.

Key words: Neuron model, neural spiking, firing rate, inhomogeneous Poisson point processes, maximum likelihood estimation

1. Introduction

Mathematical modeling applied to biological neurons has been a popular research topic for the last 50 years of neuroscience. Neuron models can fall into various categories such as compartmental, cascade, and black box models. Compartmental models include single or multiple compartmental types. The famous Hodgkin–Huxley [1] and a similar but reduced version [2] can be considered as examples of a single compartmental model. Fitzhugh–Nagumo models [3] may also be classified under the same type. One can consider [4] as an example of a multicompartmental model. These are quite complicated but realistic biophysical models. If biophysical features are not that important, one can refer to cascade models. These can be constructed from a combination of a linear filter and a nonlinearity. These generally address the computational details of the network. These are known to be studied in research related to visual systems [5–8]. These models are not expected to be as complex as compartmental models but they do involve a certain level of dynamical features. One can also discuss the black box models, which generally concentrate on the signal processing capabilities of a neuron. A considerable percent of such models have statistical features such as the probability distribution of the response given the stimulus. Examples are [9–12]. Concerning a good review on neuron modeling studies, interested readers can refer to [13].

---

*Correspondence: resat.doruk@atilim.edu.tr

Recently, different approaches in modeling are seen in the literature. It is known from [13] that the signal processing processes in a biological neuron are stochastic. This randomness comes from the stochasticity of the ion channels and synaptic processes. Some recent studies such as [14–16] concentrated on the modeling of channel noise. In addition, the flow of ions through the channels generates electromagnetic fields, which may form an electromagnetic coupling as this will modulate the membrane potential of postsynaptic neurons [17–19]. These processes are also stochastic and may contribute to the stochasticity of information processing. In [19], it was also stated that strong magnetic fields generated by the electrical system of the heart can be detrimental to its operation.

Exposure to external electromagnetic fields may be a source of exogenous disturbance to the electrical activity of a neuron [20, 21]. That will bring unexpected dynamical responses such as double coherent resonance [22].

If all the complexity above is not needed or in other words if just the signal processing capabilities are in consideration (which is a major component of computational neuroscience), other modeling options are available. These include linear-nonlinear cascades [5–7, 23–25], where a linear filter is coupled with a static nonlinear map and static feedforward [26] and dynamical recurrent neural networks [27]. Concerning the latter, we need to stress that the continuous time version of the recurrent neural network (CTRNN) should be used. It can describe the dynamics of either the membrane potential or firing rate and can be extended to any number of neurons [28].

Usage of static or dynamical neural networks in the modeling of biological neural networks is met in the literature. Some studies [29–31] concentrated on the application of a static feedforward neural network to the modeling of the auditory cortex. Static neural networks do not describe the time-dependent nature of the operation of a biological neuron (action potentials, refractory regions, etc.). Thus, dynamical recurrent neural networks seem very suitable to describe the signal processing features of a neural network. One such application was done in [32] with membrane potentials being the dynamical variables.

Continuous time recurrent neural networks have self-excitatory and/or inhibitory connections, which can be considered equivalent to an autapse that is a synaptic connection formed between parts of the same neuron (e.g., dendrites and axon). Autapse connections may recover the signal transduction in the case of a neurodegenerative disease [33, 34]. In addition, autapse connections may alter or regulate the dynamical features of a neuron [35–37].

Regardless of the model, the information transmitted is coded in successive bursts of action potentials. This is especially the case in the sensory neural transmission. This phenomenon is called neural spiking and the timing of each action potential in the burst is called a spike. The temporal locations of the spikes are believed to code the information transmitted [38] and thus may be used as time series data in identification of the neuron parameters. These facts support a theoretical neuroscientist in the following way:

If the neuron is isolated (in other words in vitro), measurement of the membrane potential will not be an issue; however, its in vivo measurement (when the neuron is alive and functional in the body) will bring many challenges. Placement of an electrode on the neuron's membrane will most probably alter its operation, so one should offer an alternate measurement approach. If an electrode is placed at a location near the neuron, one will be able to record the temporal locations of each individual action potential (and thus the neural spikes). The collected data can be used as a time series to train the model in consideration.

In [39] it was stated that neural spiking profiles of sensory neurons largely obey an inhomogeneous Poisson

process. As an inhomogeneous point process has a well-defined probability mass function as discussed in [40], an efficient way to perform parameter identification is the maximum likelihood method [41].

Identification of neuron parameters is an interesting topic in the theoretical/computational neuroscience literature. When the membrane potential or firing rate is assumed to be measurable, one can apply classical minimum mean square (or least squares) methods [42], synchronization [43], and adaptive Lyapunov+synchronization-based techniques [44]. However, in the case of this research, the collected data are discontinuous and no amplitude/rate information is available. Thus, methods in the aforementioned references are not directly applicable. Recently, there have been certain attempts to apply the concept of synchronization to spiking neurons. The problem can be roughly viewed as the synchronization of two neural spiking processes by minimizing the interspiking intervals (ISI). One example is [45], which utilizes spike synchrony monitoring [46] through minimizing the van Rossum distance [47] between two spike trains. The main issue associated with this approach is the necessity of an intermediate mechanism [48] to compute the van Rossum distance. This will be a source of increased computational complexity and thus is not preferred in this research.

In this research we will present a simulation-based study aiming at the estimation of the parameters of a firing rate-based single neuron model. One can summarize the procedure as follows:

1. Given a predefined stimulus (Fourier series, etc.), the model with true parameters will be simulated in a finite time. The firing rate profile is obtained.

2. Using a method for simulation of inhomogeneous Poisson processes, the expected spiking profile is obtained.

3. **Steps 1 and 2** should be repeated several times to obtain adequate statistics.

4. Using a maximum likelihood method, the obtained spike trains will be used to recover the model parameters.

5. Different stimuli with various configurations will be examined to obtain a sufficient amount of data for a comparison.

Studies targeting similar goals can be seen in the literature. Some examples are [29–31]. These work on a feedforward dynamical static neural network trained from neural spiking datasets. Contrary to those, we will concentrate on a simple but dynamical model (time-dependent) in this research. This is expected to be a new contribution to the related computational neuroscience literature.

2. Materials and methods
2.1. The neuron model
We are working on a single neuron model describing the firing rate dynamics [28], which is mathematically expressed as shown below:

$$\dot{r} = -ar + bg(wr + u), \tag{1}$$

where $r(t)$ is the firing rate in Hz or ($\frac{1}{s}$), $u(t)$ is the stimulus input, a is an inverse time constant in $\frac{1}{s}$, b is a maximum firing rate parameter, and w is a weight parameter. The function $g(x)$ is a parametrized logistic sigmoid function as shown below:

$$g(x) = \frac{1}{1 + exp[-c(x - h)]}, \tag{2}$$

where c is a slope and h is a soft-threshold parameter. In the above, $x = wr + u$. The true parameter values are $a = 50$, $b = 4000$, $w = 0.7$, $c = 0.04$, and $h = 70$. These parameters are to be recovered in the estimation procedure. Thus, the parameters to be estimated are $\theta = [a, b, w, c, h]$.

2.2. Stimulus

The stimulus $u(t)$ is the only input to steer the output firing rate of the neuron. Thus, it would be convenient to use a few different profiles. We are examining three different stimuli. One is a simple exponential stimulus that has no superimposed components like Forier series. The other two are complicated ones that have superimposed components. One of those will be modeled as a real Fourier series (FS) and the other will be modeled by radial basis functions (RBFs). As we will see in the following subsections, the parameters associated with stimuli are all assigned randomly from a prespecified range. That has two purposes. First of all, we will have independent stimuli in each trial, which will help increase the content of the information associated with the neuron parameters in the combined response from different trials. Secondly, in the case that this research is adapted to an experimental application, the experiment's subject should be stimulated by a different stimulus in each iteration. The reason for the latter situation is associated with the attenuated response to the same stimulus repeated more than a few times.

2.2.1. Phased cosine Fourier series (FS)

Phased cosine Fourier series are periodic functions that are mathematically expressed as shown below:

$$u(t) = \sum_{i=1}^{N_U} A_i \cos(2\pi \times i \times f_0 \times t + \phi_i), \tag{3}$$

where A_i is the amplitude and ϕ_i is the phase angle of the ith component of Eq. (3), f_0 is the base frequency of the stimulus in Hz, and N_U is the total number of its components. We said in Section 1 that the trials should be repeated for obtaining adequate statistics. In order to achieve that, the parameters A_i, ϕ_i, and f_0 can be randomly assigned. One approach is to draw a value from a uniform distribution as follows: $A_i = unifrnd(0, A_{\max})$, $\phi_i = unifrnd(-\pi, \pi)$, and $f_0 = unifrnd(0, f_{\max})$, where $unifrnd(a_1, a_2)$ yields a uniformly distributed random number in the range $[a_1, a_2]$.

2.2.2. Exponential stimulus (ES)

Exponential stimuli are very simple stimulus forms that can be expressed as follows:

$$u(t) = A\left[1 - \exp(-\alpha t)\right]. \tag{4}$$

As understood above, an exponential stimulus is not periodic. Like Eq. (3), parameters A_i and α are going to be assigned randomly per each trial. In other words, $A = unifrnd(-A_{\max}, A_{\max})$ and $\alpha = unifrnd(0, \alpha_{\max})$.

2.2.3. Radial basis functions (RBFs)

These are weighted sum of basis functions, which can mathematically be expressed as:

$$u(t) = \sum_{i=1}^{N_U} A_i \Phi(|t - t_i|), \tag{5}$$

where $\Phi(x)$ is a basis function, A_i is the amplitude of each component (a weighting factor), and t_i is the center on the time axis. $\Phi(x)$ may be in various forms and it will be assumed Gaussian here:

$$\Phi(x) = \exp[-(\epsilon x)^2], \tag{6}$$

with ϵ being a positive constant. Like Eq. (3), parameters A_i, ϵ and t_i are going to be assigned randomly in each trial. Specifically, $A_i = unifrnd(-A_{\max}, A_{\max})$, $\epsilon_i = unifrnd(0, \epsilon_{\max})$, and $t_i = unifrnd(0, T_f)$. In the latter expression, T_f is the simulation time.

2.3. Simulation of spiking

We obtain the firing rate profile $r(t)$ by integrating Eq. (1). This is in fact an auxiliary variable that is not available from direct measurement. However, as said in Section 1, one can obtain the temporal locations of individual spikes from the neuron in vivo. In a simulation, using a firing rate-based model one will be able to simulate the temporal locations of those spikes by simulating an inhomogeneous Poisson process, the probability mass function of which is shown below:

$$\text{Prob}\left[N\left(t + \Delta t\right) - N\left(t\right) = k\right] = \frac{e^{-\lambda}\lambda^k}{k!}, \tag{7}$$

where

$$\lambda = \int_t^{t+\Delta t} r_e\left(\tau\right) d\tau. \tag{8}$$

In this research, we will implement the local Bernoulli approximation of Poisson processes as described below:

1. Divide the interval of simulation $[0, T_f]$ into N_f bins each being Δt long.

2. Sample the firing rate $r(t)$ into N_f bins as $r_i = r(i\Delta t)$.

3. At instant i draw a number x_{rand} uniformly distributed between $[0, 1]$.

4. If $r_i > x_{rand}$ at $t = t_i = i\Delta t$ we will have a spike; otherwise, we will not have any spike at $t = t_i$.

5. Repeat all steps above and obtain a spike train as S.

6. For each trial k one can record the spike trains as S_k.

2.4. Likelihood methods

In Section 2.3 we presented an approach for simulating neural spiking from firing rate data. That is in fact a local Bernboulli approximation of inhomogeneous Poisson processes. Mathematically, this is:

$$\text{Probability that in } [t, t + \Delta t] = \text{a spike} \begin{cases} \text{exists: } r(t)\Delta t \\ \text{not to exist: } 1 - r(t)\Delta t, \end{cases} \tag{9}$$

with $r(t)$ being the firing rate at current instant t. A detailed explanation can be found in [40]. When Δt becomes very small or $\Delta t \to 0$, the probability density of seeing K_i spikes in the interval $[0, T_f]$ will be:

$$p(S_i) = \exp\left(-\int_0^{T_f} r(\tau)d\tau\right) \prod_{k=1}^{K_i} r(t_k). \tag{10}$$

In the above, S_i denotes the ith spike train and t_k denotes the temporal location of the kth spike in S_i. As $r(t)$ is a function of parameters θ one can rewrite the above as follows:

$$p(S_i \mid \theta) = \exp\left(-\int_0^{T_f} r(\tau, \theta)d\tau\right) \prod_{k=1}^{K_i} r(t_k, \theta). \tag{11}$$

Suppose that one has N_{it} number of independent spike trains S_i where $i = 1 \ldots N_{it}$. These can be obtained from N_{it} repeated trials. The joint likelihood function can be written as:

$$p(S_1, S_2, \ldots, S_{N_{it}} \mid \theta) = \prod_{i=1}^{N_{it}} \exp\left(-\int_0^{T_f} r_i(\tau, \theta)d\tau\right) \prod_{k=1}^{K_i} r_i(t_k, \theta). \tag{12}$$

The computation can be further simplified by taking its natural logarithm and the log-likelihood is obtained:

$$Lp(S \mid \theta) = \ln\left[(S_1, S_2, \ldots, S_{N_{it}} \mid \theta)\right] = \sum_{i=1}^{N_{it}}\left(-\int_0^{T_f} r_i(\tau, \theta)d\tau\right) \sum_{i=1}^{N_{it}}\sum_{k=1}^{K_i} \ln\left[r_i(t_k, \theta)\right], \tag{13}$$

where $r_i(t, \theta)$ is the firing rate evaluated at the current value of parameter θ. The maximum likelihood estimate (MLE) of parameter θ can be found by:

$$\hat{\theta}_{ML} = \arg\max_{\theta}\left[Lp(S \mid \theta)\right]. \tag{14}$$

3. Example application

In this section we will utilize the theory presented to estimate the parameters (θ) of the model in Eq. (1).

3.1. Response to particular stimuli

It will be convenient to see how the neuron in Eq. (1) with the nominal values of its parameters in Section 2.1 responds to the stimuli defined in Section 2.2. One can see a typical example for a Fourier series and exponential and radial basis function stimuli and their associated responses from the neuron in Figures 1a–1c, respectively.

3.2. Simulation details

In this work our goal is to estimate all parameters from Eqs. (1) and (2), which are $\theta = [a, b, w, c, h]$, respectively. Their true values are given in Section 2.1. The working principles in the example problem can be described in a step-by-step fashion as shown below:

1. A single run of simulation will last for $T_f = 3$ s.

2. The neuron model in Eq. (1) will be simulated at the true value of parameters given in Section 2.1 and firing rate data are stored as $r_m(t)$ where m is the current iteration number. At each iteration, the stimulus parameters in Eqs. (3), (4), and (5) should be modified. In Section 2.2 we discussed three different stimuli and indicated that their parameters are assigned randomly from a uniform distribution.

3. Firing rate data $r_m(t)$ are used to generate neural spikes S_m in the mth run using the methodology defined in Section 2.3. These data will be used to compute the likelihood. The number of spikes will be K_m at the mth run.
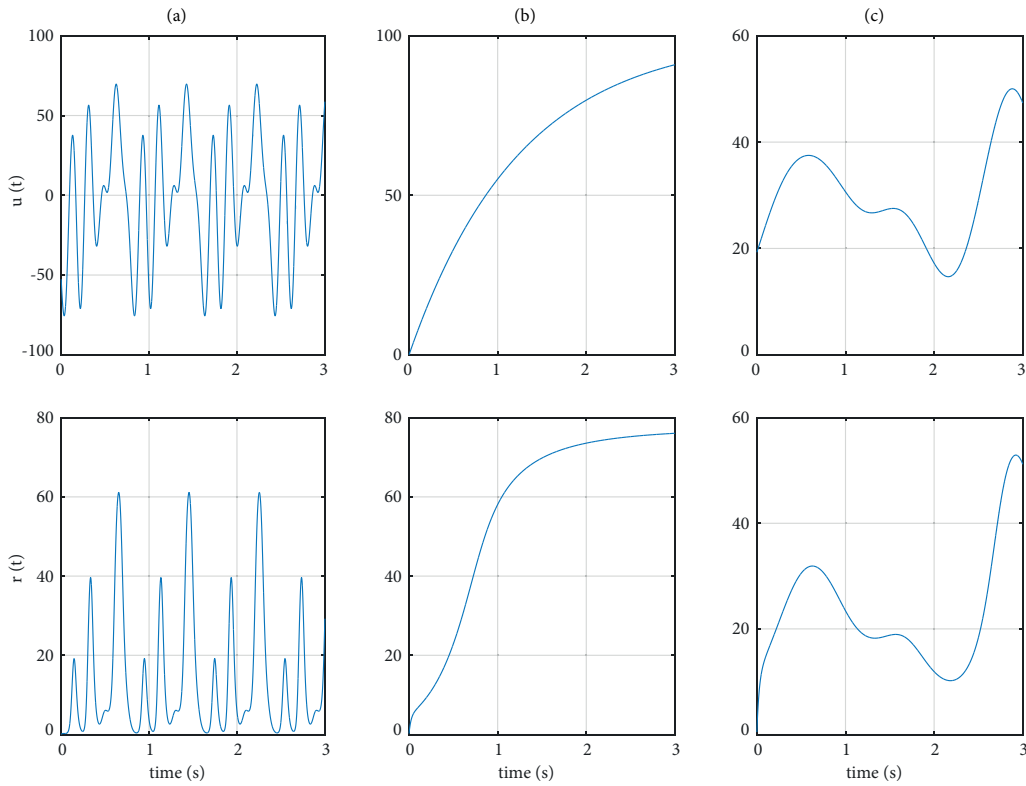
Figure. The response of the neuron in Eq. (1) to stimuli defined in Section 2.2. First row has the stimuli whereas second has the responses. a) Fourier series stimulus (Section 2.2.1) with amplitude $A_i = 25$, $f_0 = 1.25$ Hz, and phases uniformly distributed between $[-\pi, \pi]$ radians. $N_U = 5$. b) Exponential stimulus (Section 2.2.2) with amplitude $A = 100$ and slope $\alpha = 0.8$. c) Radial basis function stimulus (Section 2.2.3) with $A_i = 25$, $\epsilon = 2$, and t_i ordered and randomly assigned from a set uniformly distributed in the range $[0, T_f]$.

4. Repeat the simulation N_{it} times to obtain a large set of independent spikes (so that broader statistical information content is obtained).

5. The spiking data needed by Eq. (13) will be obtained at the 4th step. However, the firing rate component of Eq. (13) should be computed at the current iteration of the optimization.

6. Run an optimization algorithm that computes the firing rate at the current iterated value of the parameters but the spikes from **Step 4**.

The nominal data associated with the current problem are given in Table 1. The table presents all varied data describing the performed simulations.

3.3. Presentation of the results
In this section, the results of the parameter estimation study are presented. The tabulated data will show the variation of mean estimated values $\hat{\theta} = [\hat{a}, \hat{b}, \hat{w}, \hat{c}, \hat{h}]$ of parameters $\theta = [a, b, w, c, h]$, percent estimation errors $\Delta_i = 100\frac{\theta_i - \hat{\theta}_i}{\theta_i}$, and standard deviation of the estimates ($\sigma_i = \sigma(\hat{\theta}_i)$) against relevant varying stimulus parameters. Results are grouped according to the stimulus type (Fourier series, Eq. (3); exponential, Eq. (4); or radial basis functions, Eq. (5)).

Table 1. Typical data related to the simulation scenario. In the case that there are multiple values associated with each parameter, all of them are presented in the table. If a parameter is associated with one or more stimuli then relevant equation number(s) are indicated next to the definition of the parameter.

Parameter	Symbol	Value
Simulation time	T_f	3 s
Number of trials	N_{it}	25, 50, 100, 200, 400
# of components in stimulus [(3) and (5)]	N_U	5, 10, 20, 30, 40, 50
Method of optimization	N/A	Interior-point gradient descent (MATLAB)
# of true parameters	Size(θ)	5
Maximum stimulus amplitude	$A_{\max}$	25, 50, 100, 200, 400
Maximum base frequency [(3)]	$f_{\max}$	1, 2, 5, 10, 20 Hz
Maximum value of parameter α [(4)]	$\alpha_{\max}$	0.1, 0.2, 0.5, 1, 2, 5, 10
Maximum value of parameter ϵ [(5)]	$\epsilon_{\max}$	0.1, 0.2, 0.5, 1, 2

3.3.1. Results of estimation under Fourier series stimulation (Tables 2a–h)

The variation of the mean estimated values are shown in Table 2a (versus sample size N_{it}), in Table 2c (versus stimulus component count N_U), in Table 2e (versus maximum amplitude $A_{\max}$), and in Table 2g (versus the maximum base frequency $f_{\max}$).

The variation of the standard deviation and percent errors of estimates are shown in Table 2b (versus sample size N_{it}), in Table 2d (versus stimulus component count N_U), in Table 2f (versus maximum amplitude $A_{\max}$), and in Table 2h (versus the maximum base frequency $f_{\max}$).

3.3.2. Results of estimation under exponential stimulation (Tables 3a–3f)

The variation of the mean estimated values are shown in Table 3a (versus sample size N_{it}), in Table 3c (versus maximum amplitude $A_{\max}$), and in Table 3e (versus parameter α_{max}).

The variation of the mean estimated values are shown in Table 3b (versus sample size N_{it}), in Table 3d (versus maximum amplitude $A_{\max}$), and in Table 3f (versus parameter α_{max}).

3.3.3. Results of estimation under radial basis function stimulation (Tables 4a–4h)

The variation of the mean estimated values are shown in Table 4a (versus sample size N_{it}), in Table 4c (versus stimulus component count N_U), in Table 4e (versus maximum amplitude $A_{\max}$), and in Table 4g (versus parameter $\epsilon_{\max}$).

The variation of the standard deviation and percent errors of estimates are shown in Table 4b (versus sample size N_{it}), in Table 4d (versus stimulus component count N_U), in Table 4f (versus maximum amplitude $A_{\max}$), and in Table 4h (versus the maximum exponential decay limit $\epsilon_{\max}$).

4. Discussion and conclusion
4.1. Evaluation of this research
In this paper, we performed a theoretical study aiming at input-output modeling of a single neuron from discrete neural spiking data. The model of Eq. (1) receives an external stimulus $u(t)$ and generates the instantaneous firing rate $r(t)$ of the neuron. As one does not have a continuous set of data, one will not be able to implement neural network training algorithms such as minimum mean square estimation (MMSE). Knowing that neural spiking events obey an inhomogeneous Poisson process (driven by the firing rate of the neuron in

Table 2. The variation of the mean estimated values $(\hat{a}, \hat{b}, \hat{w}, \hat{c}, \hat{h})$ of the parameters in Eqs. (1) and (2), their associated standard deviations $[\sigma_a, \sigma_b, \sigma_w, \sigma_c, \sigma_h]$, and percent estimation errors $[\Delta_a, \Delta_b, \Delta_w, \Delta_c, \Delta_h]$ varying against increasing sample size N_{it}, stimulus component count N_U, maximum amplitude $A_{\max}$, and maximum base frequency limit $f_{\max}$. The simulation is performed under Fourier series stimulation as shown in Eq. (3). The variation is shown in column-wise order. The test conditions are described in the relevant subtables.

(a) Estimated value vs. N_{it} ($N_U = 5$, $A_{\max} = 100$, $f_{\max} = 5$)

N_{it}	$\hat{a}$	$\hat{b}$	$\hat{w}$	$\hat{c}$	$\hat{h}$
25	49.6702	3962.26	0.713055	0.0404492	69.8123
50	49.7277	3947.2	0.699566	0.0408769	69.2398
100	49.5803	3952.05	0.692783	0.0407338	69.2864
200	49.8278	3985.21	0.697807	0.0402862	69.8498
400	49.8216	3979.05	0.685709	0.040575	69.2888

(b) Standard deviations and percent errors vs. N_{it} ($N_U = 5$, $A_{\max} = 100$, $f_{\max} = 5$)

N_{it}	σ_a	σ_b	σ_w	σ_c	σ_h	Δ_a %	Δ_b %	Δ_w %	Δ_c %	Δ_h %
25	3.2523	250.25	0.14982	0.003113	4.4974	0.65963	0.94344	1.8651	1.123	0.26812
50	1.93	169.95	0.12203	0.0030545	4.4771	0.54461	1.32	0.06205	2.1924	1.086
100	1.6148	143.73	0.10262	0.0020419	3.426	0.83947	1.1988	1.031	1.8346	1.0195
200	1.2223	109.96	0.067439	0.0014433	2.2846	0.34442	0.36975	0.31327	0.7156	0.21459
400	0.81524	77.634	0.040126	0.0011569	1.5265	0.35688	0.52364	2.0416	1.4374	1.016

(c) Estimated value vs. N_U ($N_{it} = 100$, $A_{\max} = 100$, $f_{\max} = 5$)

N_U	$\hat{a}$	$\hat{b}$	$\hat{w}$	$\hat{c}$	$\hat{h}$
5	49.5803	3952.05	0.692783	0.0407338	69.2864
10	50.0618	4021.98	0.737201	0.0389883	72.1104
20	50.2957	4011.24	0.696211	0.0412647	69.2391
30	49.9352	4009.47	0.745973	0.0403041	72.1552
40	49.7945	4004.43	0.691043	0.0443499	70.4688
50	50.062	3996.12	0.650736	0.0441861	67.2971

(d) Standard deviations and percent errors vs. N_U ($N_{it} = 100$, $A_{\max} = 100$, $f_{\max} = 5$)

N_U	σ_a	σ_b	σ_w	σ_c	σ_h	Δ_a %	Δ_b %	Δ_w %	Δ_c %	Δ_h %
5	1.6148	143.73	0.10262	0.0020419	3.426	0.83947	1.1988	1.031	1.8346	1.0195
10	1.2628	113.85	0.080338	0.0020276	2.8458	0.1236	0.54953	5.3145	2.5293	3.0149
20	1.4673	137.45	0.11413	0.005243	5.6506	0.59134	0.28103	0.54135	3.1618	1.087
30	1.6828	125.26	0.16482	0.0050525	4.9211	0.12962	0.23669	6.5676	0.76025	3.0788
40	1.3203	124.3	0.20294	0.0075247	6.9202	0.41096	0.11065	1.2796	10.875	0.6697
50	1.8944	136.79	0.18859	0.0082924	7.6774	0.12399	0.096927	7.0377	10.465	3.8612

(e) Estimated value vs. $A_{\max}$ ($N_{it} = 100$, $N_U = 5$, $f_{\max} = 5$)

$A_{\max}$	$\hat{a}$	$\hat{b}$	$\hat{w}$	$\hat{c}$	$\hat{h}$
25	49.4921	3884.35	0.730901	0.0404005	69.0571
50	49.5848	3921.27	0.707979	0.0404341	69.3344
100	49.5803	3952.05	0.692783	0.0407338	69.2864
200	49.6737	3970.31	0.68331	0.0411265	69.2959
400	49.8511	3986.75	0.669525	0.042103	69.0208

(f) Standard deviations and percent errors vs. $A_{\max}$ ($N_{it} = 100$, $N_U = 5$, $f_{\max} = 5$)

$A_{\max}$	σ_a	σ_b	σ_w	σ_c	σ_h	Δ_a %	Δ_b %	Δ_w %	Δ_c %	Δ_h %
25	3.6609	753.82	0.17617	0.0026882	7.0928	1.0158	2.8913	4.4144	1.0012	1.3471
50	1.3613	168.99	0.064836	0.0016451	2.8031	0.83045	1.9682	1.1399	1.0852	0.95092
100	1.6148	143.73	0.10262	0.0020419	3.426	0.83947	1.1988	1.031	1.8346	1.0195
200	1.2751	103.02	0.10666	0.0026259	4.0119	0.65263	0.74219	2.3842	2.8163	1.0058
400	1.0805	86.904	0.13438	0.0041455	5.3532	0.29771	0.33133	4.3536	5.2576	1.3988

(g) Estimated value vs. $f_{\max}$ ($N_{it} = 100$, $N_U = 5$, $A_{\max} = 100$)

$f_{\max}$	$\hat{a}$	$\hat{b}$	$\hat{w}$	$\hat{c}$	$\hat{h}$
1	49.407	3947.7	0.682244	0.0406495	69.1084
2	50.2906	4018.33	0.714426	0.0399609	70.3308
5	49.5803	3952.05	0.692783	0.0407338	69.2864
10	50.0735	4005.05	0.711637	0.040597	70.2946
20	49.9281	3984.12	0.695925	0.0410583	69.507

(h) Standard deviations and percent errors vs. $f_{\max}$ ($N_{it} = 100$, $N_U = 5$, $A_{\max} = 100$)

$f_{\max}$	σ_a	σ_b	σ_w	σ_c	σ_h	Δ_a %	Δ_b %	Δ_w %	Δ_c %	Δ_h %
1	2.3076	177.21	0.10161	0.0022874	3.8233	1.1861	1.3074	2.5366	1.6238	1.2737
2	1.9963	152.46	0.071988	0.0018978	2.7653	0.58122	0.45823	2.0609	0.097849	0.47261
5	1.6148	143.73	0.10262	0.0020419	3.426	0.83947	1.1988	1.031	1.8346	1.0195
10	1.3089	133.4	0.088437	0.0024846	3.2786	0.14693	0.12615	1.6625	1.4925	0.42088
20	1.7063	147.19	0.089058	0.0021409	2.9289	0.14378	0.39702	0.58207	2.6458	0.70427

Table 3. The variation of the mean estimated values $(\hat{a}, \hat{b}, \hat{w}, \hat{c}, \hat{h})$ of the parameters in Eqs. (1) and (2), their associated standard deviations $[\sigma_a, \sigma_b, \sigma_w, \sigma_c, \sigma_h]$, and percent estimation errors $[\Delta_a, \Delta_b, \Delta_w, \Delta_c, \Delta_h]$ varying against increasing sample size N_{it}, maximum amplitude $A_{\max}$, and maximum decay limit $\alpha_{\max}$. The simulation is performed under exponential stimulation as shown in Eq. (4). The variation is shown in column-wise order. The test conditions are described in the relevant subtables.

(a) Estimated value vs. N_{it} ($\alpha_{\max} = 1$, $A_{\max} = 100$)

N_{it}	$\hat{a}$	$\hat{b}$	$\hat{w}$	$\hat{c}$	$\hat{h}$
25	55.4146	4584.33	0.687265	0.0408969	69.843
50	46.3121	3782.76	0.683699	0.0407907	69.4424
100	50.7409	4164.19	0.693567	0.0401297	70.3082
200	42.3099	3383.26	0.699526	0.0401604	69.7471
400	41.8393	3312.65	0.710735	0.0401126	69.6292

(b) Standard deviations and percent errors vs. N_{it} ($\alpha_{\max} = 1$, $A_{\max} = 100$)

N_{it}	σ_a	σ_b	σ_w	σ_c	σ_h	Δ_a %	Δ_b %	Δ_w %	Δ_c %	Δ_h %
25	33.576	2780.2	0.29593	0.0047745	8.8051	10.829	14.608	1.8193	2.2422	0.22436
50	27.174	2321	0.20602	0.0034566	6.0301	7.3757	5.4311	2.3288	1.9767	0.79662
100	21.275	1870	0.14486	0.0022326	3.6764	1.4817	4.1047	0.91903	0.32427	0.44035
200	14.448	1153.6	0.098932	0.001727	2.993	15.38	15.418	0.067761	0.40091	0.36131
400	8.9178	681.02	0.063656	0.0011323	1.9523	16.321	17.184	1.5335	0.28149	0.52971

(c) Estimated value vs. $A_{\max}$ ($\alpha_{\max} = 1$, $N_{it} = 100$)

$A_{\max}$	$\hat{a}$	$\hat{b}$	$\hat{w}$	$\hat{c}$	$\hat{h}$
25	50.6207	4724.06	0.778068	0.0422222	71.3822
50	51.3891	4542.35	0.798141	0.0396399	72.6516
100	50.7409	4164.19	0.693567	0.0401297	70.3082
200	50.3099	4044.74	0.661934	0.0409667	68.6142
400	45.6164	3653.08	0.637799	0.0415122	67.5289

(d) Standard deviations and percent errors vs. $A_{\max}$ ($\alpha_{\max} = 1$, $N_{it} = 100$)

$A_{\max}$	σ_a	σ_b	σ_w	σ_c	σ_h	Δ_a %	Δ_b %	Δ_w %	Δ_c %	Δ_h %
25	25.526	2812.3	0.62184	0.0085827	34.759	1.2414	18.102	11.153	5.5556	1.9745
50	24.95	2202.1	0.39529	0.0028729	10.685	2.7782	13.559	14.02	0.90014	3.7881
100	21.275	1870	0.14486	0.0022326	3.6764	1.4817	4.1047	0.91903	0.32427	0.44035
200	18.043	1487.2	0.11115	0.0023031	4.242	0.61984	1.1186	5.4381	2.4167	1.9797
400	15.264	1240.4	0.1398	0.0026473	4.903	8.7672	8.673	8.8858	3.7806	3.5301

(e) Estimated value vs. $\alpha_{\max}$ ($A_{\max} = 100$, $N_{it} = 100$)

$\alpha_{\max}$	$\hat{a}$	$\hat{b}$	$\hat{w}$	$\hat{c}$	$\hat{h}$
0.1	51.6784	4643.79	0.809648	0.0436627	70.8784
0.2	51.5378	4868.04	0.781444	0.040371	73.8027
0.5	51.3628	4172.82	0.724197	0.0399298	70.6699
1	50.7409	4164.19	0.693567	0.0401297	70.3082
2	49.8163	4023.17	0.667447	0.0407077	69.133
5	47.3915	3790.83	0.668843	0.0408237	68.7438
10	46.0624	3687.45	0.675668	0.040657	68.9123

(f) Standard deviations and percent errors vs. $\alpha_{\max}$ ($A_{\max} = 100$, $N_{it} = 100$)

$\alpha_{\max}$	σ_a	σ_b	σ_w	σ_c	σ_h	Δ_a %	Δ_b %	Δ_w %	Δ_c %	Δ_h %
0.1	26.546	2753	0.57792	0.012047	37.267	3.3568	16.095	15.664	9.1567	1.2549
0.2	27.461	2306.2	0.51004	0.0045518	17.032	3.0756	21.701	11.635	0.92758	5.4324
0.5	23.97	1981.3	0.19326	0.0026688	4.6969	2.7256	4.3205	3.4567	0.17539	0.95704
1	21.275	1870	0.14486	0.0022326	3.6764	1.4817	4.1047	0.91903	0.32427	0.44035
2	19.494	1593.7	0.14595	0.0024702	4.5219	0.36749	0.57914	4.6504	1.7692	1.2386
5	16.986	1343.5	0.11264	0.0021599	3.8037	5.217	5.2293	4.451	2.0594	1.7946
10	13.461	1099	0.12594	0.002484	4.4121	7.8752	7.8137	3.476	1.6424	1.5539

consideration), point process likelihood functions can be derived for a maximum likelihood estimation procedure. In this research, we compare the results of a maximum likelihood estimation of the neuron model stimulated by three different stimuli. Those are modeled by a phase cosine Fourier series (Eq. (3)), by exponential functions (Eq. (4)), and by radial basis functions (Eq. (5)). In order to evaluate the performance of our methodologies

Table 4. The variation of the mean estimated values $(\hat{a}, \hat{b}, \hat{w}, \hat{c}, \hat{h})$ of the parameters in Eq. (1) and (2), their associated standard deviations $[\sigma_a, \sigma_b, \sigma_w, \sigma_c, \sigma_h]$, and percent estimation errors $[\Delta_a, \Delta_b, \Delta_w, \Delta_c, \Delta_h]$ varying against increasing sample size N_{it}, stimulus component count N_U, maximum amplitude $A_{\max}$, and maximum exponential decay limit $\epsilon_{\max}$. The simulation is performed under radial basis stimulation as shown in Eq. (5). The variation is shown in column-wise order. The test conditions are described in the relevant subtables.

(a) Estimated value vs. N_{it} $(\epsilon_{\max} = 1,\ A_{\max} = 100,\ N_U = 5)$

N_{it}	$\hat{a}$	$\hat{b}$	$\hat{w}$	$\hat{c}$	$\hat{h}$
25	47.4994	3786.42	0.623158	0.0432567	66.8859
50	46.8557	3736.35	0.630123	0.0422188	67.2313
100	47.7897	3807.87	0.666921	0.0411835	68.2491
200	48.376	3866.56	0.687372	0.0404378	69.3467
400	48.192	3859.11	0.67995	0.0404762	69.2331

(b) Standard deviations and percent errors vs. N_{it} $(\epsilon_{\max} = 1,\ A_{\max} = 100,\ N_U = 5)$

N_{it}	σ_a	σ_b	σ_w	σ_c	σ_h	Δ_a %	Δ_b %	Δ_w %	Δ_c %	Δ_h %
25	16.568	1335	0.27757	0.0063837	10.563	5.0012	5.3396	10.977	8.1418	4.4487
50	8.1304	659.67	0.1423	0.0038269	5.8373	6.2887	6.5913	9.9824	5.547	3.9553
100	7.3164	579.78	0.096433	0.0022259	3.5297	4.4207	4.8032	4.7255	2.9587	2.5013
200	4.8891	399.2	0.06561	0.0018656	2.6633	3.248	3.3359	1.804	1.0945	0.93332
400	3.2943	259.34	0.045889	0.0011839	1.8678	3.6161	3.5222	2.8643	1.1905	1.0956

(c) Estimated value vs. N_U $(\epsilon_{\max} = 1,\ N_{it} = 100,\ A_{\max} = 100)$

N_U	$\hat{a}$	$\hat{b}$	$\hat{w}$	$\hat{c}$	$\hat{h}$
5	47.7897	3807.87	0.666921	0.0411835	68.2491
10	50.1875	3993.74	0.706247	0.0403806	69.7851
20	54.1888	4324.32	0.672623	0.0408096	69.025
30	51.0134	4073.77	0.715367	0.0400908	70.7323
40	54.7428	4371.69	0.724818	0.0397978	70.8009
50	49.2361	3935.07	0.672783	0.0409923	69.5051

(d) Standard deviations and percent errors vs. N_U $(\epsilon_{\max} = 1,\ N_{it} = 100,\ A_{\max} = 100)$

N_U	σ_a	σ_b	σ_w	σ_c	σ_h	Δ_a %	Δ_b %	Δ_w %	Δ_c %	Δ_h %
5	7.3164	579.78	0.096433	0.0022259	3.5297	4.4207	4.8032	4.7255	2.9587	2.5013
10	9.7434	758	0.13708	0.0027047	5.4608	0.375	0.15649	0.89244	0.95143	0.30706
20	8.0929	648.87	0.10876	0.0026352	4.3537	8.3777	8.1081	3.911	2.0239	1.3929
30	6.5797	516.32	0.12683	0.0024758	4.8838	2.0267	1.8442	2.1953	0.22704	1.0461
40	9.1035	708.08	0.13055	0.0024886	5.2001	9.4856	9.2923	3.5454	0.50539	1.1441
50	6.9541	554.97	0.13048	0.0028784	4.8343	1.5278	1.6232	3.8882	2.4808	0.70705

(e) Estimated value vs. $A_{\max}$ $(\epsilon_{\max} = 1,\ N_{it} = 100,\ N_U = 5)$

$A_{\max}$	$\hat{a}$	$\hat{b}$	$\hat{w}$	$\hat{c}$	$\hat{h}$
25	52.5307	4551.35	0.662925	0.0404999	71.2279
50	49.9751	3998	0.676728	0.0406683	69.1362
100	47.7897	3807.87	0.666921	0.0411835	68.2491
200	46.685	3729.4	0.643105	0.0415325	67.5437
400	48.6872	3885.46	0.62935	0.0424042	66.771

(f) Standard deviations and percent errors vs. $A_{\max}$ $(\epsilon_{\max} = 1,\ N_{it} = 100,\ N_U = 5)$

$A_{\max}$	σ_a	σ_b	σ_w	σ_c	σ_h	Δ_a %	Δ_b %	Δ_w %	Δ_c %	Δ_h %
25	17.935	1506.5	0.2107	0.0027386	5.571	5.0614	13.784	5.2964	1.2499	1.7541
50	11.047	882.24	0.13237	0.0029216	5.0519	0.049768	0.050047	3.3246	1.6707	1.234
100	7.3164	579.78	0.096433	0.0022259	3.5297	4.4207	4.8032	4.7255	2.9587	2.5013
200	5.952	470.71	0.12241	0.0027892	4.9509	6.63	6.7649	8.1278	3.8312	3.509
400	6.0185	478.06	0.21211	0.0052963	8.6267	2.6256	2.8636	10.093	6.0105	4.6129

(g) Estimated value vs. $\alpha_{\max}$ $(A_{\max} = 100,\ N_{it} = 100,\ N_U = 5)$

$\epsilon_{\max}$	$\hat{a}$	$\hat{b}$	$\hat{w}$	$\hat{c}$	$\hat{h}$
0.1	46.6119	3726.73	0.670111	0.0408556	68.759
0.2	46.5827	3726.27	0.667673	0.0409112	68.6946
0.5	47.7759	3819.34	0.701089	0.0402121	69.9108
1	47.7897	3807.87	0.666921	0.0411835	68.2491
2	51.692	4123.9	0.713619	0.0400674	70.3015
5	50.1343	4002.4	0.701113	0.0401714	69.8546

(h) Standard deviations and percent errors vs. $\alpha_{\max}$ $(A_{\max} = 100,\ N_{it} = 100,\ N_U = 5)$

$\epsilon_{\max}$	σ_a	σ_b	σ_w	σ_c	σ_h	Δ_a %	Δ_b %	Δ_w %	Δ_c %	Δ_h %
0.1	9.1783	723.5	0.082712	0.0023445	3.5077	6.7761	6.8317	4.2699	2.139	1.7729
0.2	9.2347	731.65	0.086881	0.0024571	3.7252	6.8346	6.8432	4.6181	2.278	1.8649
0.5	8.1156	641.87	0.096607	0.002191	3.8242	4.4481	4.5165	0.15555	0.53015	0.12749
1	7.3164	579.78	0.096433	0.0022259	3.5297	4.4207	4.8032	4.7255	2.9587	2.5013
2	8.6288	679.33	0.12459	0.0027523	4.8754	3.384	3.0975	1.9455	0.16848	0.43076
5	6.8289	552.16	0.11242	0.0022092	4.0536	0.26858	0.059928	0.15901	0.42845	0.20766

we repeated the simulations with different sample sizes N_{it} and various stimulus parameters such as stimulus component counts N_U, maximum amplitude $A_{\max}$, maximum exponential decay $\alpha_{\max}$, and maximum value of the RBF parameter $\epsilon_{\max}$. The obtained results can be summarized as shown below:

1. Regardless of the stimulus, standard deviations (or variances) of the estimates have a decreasing behavior with increasing sample size N_{it}. There are no such definite patterns for percent estimation errors (Tables 2b, 3b, and 4b).

2. In simulations where stimuli are modeled by Fourier series and radial basis functions, the stimulus component count N_U does not seem to have a considerable effect on the estimation performance (Tables 2d and 4d).

3. For Fourier series stimulus, it appears that base frequencies lower than 5 Hz can generate slightly lower variance estimates; however, there is no considerable influence (Table 2h).

4. Regardless of the stimulus type, increasing the maximum amplitude parameter $A_{\max}$ leads to a moderate level of improvement of the estimation performance (variance decreases). However, this situation changes when $A_{\max}$ exceeds the 100–200 range (Tables 2f, 3d, and 4e).

5. In the simulations that involve exponential stimuli, the maximum value of exponential decay parameter $\alpha_{\max}$ also has a moderate effect on the estimation performance. Results suggest that it should be 5 or lower (Table 3f).

6. In the radial basis function stimulated cases, the $\epsilon_{\max}$ parameter also has a moderate improvement on the estimation performance. As it increases, the variances of the estimates slightly decrease (Table 4g).

7. Overall, among three different stimuli, the smallest variance of the estimates is obtained when a Fourier series stimulus is used in the estimation procedure. This can be understood when the standard deviations are compared from the tables.

4.2. Future work
It would be interesting to extend the approaches presented in this work to different types of models. One example may be the utilization of this research in the parametric identification of the Hindmarsh–Rose model [49]. That generates a series of bursts depending on the current injected (input). After a certain level of current injection, the Hindmarsh–Rose model will be trapped in a Hopf bifurcation [50] condition and repetitive bursts will appear. The frequency of bursting will depend on the injected current, so a slowly varying current will yield a frequency modulation. If noise corrupts the input, individual action potentials will appear at random locations. If the temporal locations of the peaks of those action potentials are recorded, these can form neural spiking data and the method presented in Section 2.4 can be applied to identify the parameters of an Hindmarsh–Rose model (at least partially). Studies working on a similar idea seem very limited in the literature. Thus, this should be an interesting new project. In addition, a Hindmarsh–Rose model with that setting can be used as a data generator for other models, e.g., a more complicated version of the model in Eq. (1).

References

[1] Hodgkin AL, Huxley AF. A quantitative description of membrane current and its application to conduction and excitation in nerve. J Physiol-London 1952; 117: 500-544.

[2] Morris C, Lecar H. Voltage oscillations in the barnacle giant muscle fiber. Biophys J 1981; 35: 193-213.

[3] FitzHugh R. Impulses and physiological states in theoretical models of nerve membrane. Biophys J 1961; 1: 445-466.

[4] Booth V, Rinzel J, Kiehn O. Compartmental model of vertebrate motoneurons for Ca2+-dependent spiking and plateau potentials under pharmacological treatment. J Neurophysiol 1997; 78: 3371-3385.

[5] Mante V, Frazor RA, Bonin V, Geisler WS, Carandini M. Independence of luminance and contrast in natural scenes and in the early visual system. Nat Neurosci 2005; 8: 1690-1697.

[6] Hosoya T, Baccus SA, Meister M. Dynamic predictive coding by the retina. Nature 2005; 436: 71-77.

[7] Rust NC, Schwartz O, Movshon JA, Simoncelli EP. Spatiotemporal elements of macaque v1 receptive fields. Neuron 2005; 46: 945-956.

[8] Adelson EH, Bergen JR. Spatiotemporal energy models for the perception of motion. J Opt Soc Am A 1985; 2: 284-299.

[9] Borst A, Theunissen FE. Information theory and neural coding. Nat Neurosci 1999; 2: 947-957.

[10] Barlow H. Possible principles underlying the transformation of sensory messages. In: Rosenblith W, editor. Sensory Communication. Cambridge, MA, USA: MIT Press, 1959. pp. 217-234.

[11] Fairhall AL, Lewen GD, Bialek W, van Steveninck RRdR. Efficiency and ambiguity in an adaptive neural code. Nature 2001; 412: 787-792.

[12] Hassenstein B, Reichardt W. Systemtheoretische Analyse der Zeit-, Reihenfolgen- und Vorzeichenauswertung bei der Bewegungsperzeption des Rüsselkäfers Chlorophanus. Z Naturforsch B 1956; 11: 513-524 (in German).

[13] Herz AV, Gollisch T, Machens CK, Jaeger D. Modeling single-neuron dynamics and computations: a balance of detail and abstraction. Science 2006; 314: 80-85.

[14] Ma J, Tang J. A review for dynamics in neuron and neuronal network. Nonlinear Dynam 2017; 89: 1569-1578.

[15] Linaro D, Storace M, Giugliano M. Accurate and fast simulation of channel noise in conductance-based model neurons by diffusion approximation. PLoS Comput Biol 2011; 7: e1001102.

[16] White JA, Rubinstein JT, Kay AR. Channel noise in neurons. Trends Neurosci 2000; 23: 131-137.

[17] Lv M, Wang C, Ren G, Ma J, Song X. Model of electrical activity in a neuron under magnetic flow effect. Nonlinear Dynam 2016; 85: 1479-1490.

[18] Lv M, Ma J. Multiple modes of electrical activities in a new neuron model under electromagnetic radiation. Neurocomputing 2016; 205: 375-381.

[19] Wu F, Wang C, Xu Y, Ma J. Model of electrical activity in cardiac tissue under electromagnetic induction. Sci Rep-UK 2016; 6: 28.

[20] Wang Y, Ma J, Xu Y, Wu F, Zhou P. The electrical activity of neurons subject to electromagnetic induction and Gaussian white noise. Int J Bifurcat Chaos 2017; 27: 1750030.

[21] Zhan F, Liu S. Response of electrical activity in an improved neuron model under electromagnetic radiation and noise. Front Comput Neurosc 2017; 11: 107.

[22] Wu F, Wang C, Jin W, Ma J. Dynamical responses in a new neuron model subjected to electromagnetic induction and phase noise. Physica A 2017; 469: 81-88.

[23] Chichilnisky E. A simple white noise analysis of neuronal light responses. Network-Comp Neural 2001; 12: 199-213.

[24] Paninski L. Estimation of entropy and mutual information. Neural Comput 2003; 15: 1191-1253.

[25] Sharpee TO, Sugihara H, Kurgansky AV, Rebrik SP, Stryker MP, Miller KD. Adaptive filtering enhances information transmission in visual cortex. Nature 2006; 439: 936-942.

[26] Haykin S. Neural Netwoks: A Comprehensive Foundation. 2nd ed. Upper Saddle River, NJ, USA: Prentice Hall, 2004.

[27] Funahashi Ki, Nakamura Y. Approximation of dynamical systems by continuous time recurrent neural networks. Neural Networks 1993; 6: 801-806.

[28] Miller KD, Fumarola F. Mathematical equivalence of two common forms of firing rate models of neural networks. Neural Comput 2012; 24: 25-31.

[29] DiMattina C, Zhang K. Adaptive stimulus optimization for sensory systems neuroscience. Front Neural Circuit 2013; 7: 101.

[30] DiMattina C, Zhang K. Active data collection for efficient estimation and comparison of nonlinear neural models. Neural Comput 2011; 23: 2242-2288.

[31] DiMattina C, Zhang K. How to modify a neural network gradually without changing its input-output functionality. Neural Comput 2010; 22: 1-47.

[32] Doruk RO, Zhang K. Fitting of dynamic recurrent neural network models to sensory stimulus-response data. J Biol Phys 2018; 44: 449-469.

[33] Wang C, Guo S, Xu Y, Ma J, Tang J, Alzahrani F, Hobiny A. Formation of autapse connected to neuron and its biological function. Complexity 2017; 2017: 5436737.

[34] Guo S, Wang C, Ma J, Jin W. Transmission of blocked electric pulses in a cable neuron model by using an electric field. Neurocomputing 2016; 216: 627-637.

[35] Xu Y, Ying H, Jia Y, Ma J, Hayat T. Autaptic regulation of electrical activities in neuron under electromagnetic induction. Sci Rep-UK 2017; 7: 43452.

[36] Ren G, Zhou P, Ma J, Cai N, Alsaedi A, Ahmad B. Dynamical response of electrical activities in digital neuron circuit driven by autapse. Int J Bifurcat Chaos 2017; 27: 1750187.

[37] Jia B. Negative Feedback Mediated by Fast Inhibitory Autapse Enhances Neuronal Oscillations Near a Hopf Bifurcation Point. Int J Bifurcat Chaos 2018; 28: 1850030.

[38] Dayan P, Abbott LF. Theoretical Neuroscience. 1st ed. Cambridge, MA, USA: MIT Press, 2001.

[39] Shadlen MN, Newsome WT. Noise, neural codes and cortical organization. Curr Opin Neurobiol 1994; 4: 569-579.

[40] Eden UT. Point process models for neural spike trains. In: Mitra P, editor. Neural Signal Processing: Quantitative Analysis of Neural Activity. Washington, DC, USA: Society for Neuroscience, 2008. pp. 45-51.

[41] Myung IJ. Tutorial on maximum likelihood estimation. J Math Psychol 2003; 47: 90-100.

[42] Kollias S, Anastassiou D. An adaptive least squares algorithm for the efficient training of artificial neural networks. IEEE T Circuits Syst 1989; 36: 1092-1101.

[43] Parlitz U, Junge L, Kocarev L. Synchronization-based parameter estimation from time series. Phys Rev E 1996; 54: 6253-6259.

[44] Wang CN, Ma J, Jin WY. Identification of parameters with different orders of magnitude in chaotic systems. Dynam Syst 2012; 27: 253-270.

[45] Lynch EP, Houghton CJ. Parameter estimation of neuron models using in-vitro and in-vivo electrophysiological data. Front Neuroinform 2015; 9: 10.

[46] Kreuz T, Chicharro D, Houghton C, Andrzejak RG, Mormann F. Monitoring spike train synchrony. J Neurophysiol 2012; 109: 1457-1472.

[47] van Rossum M. A novel spike distance. Neural Comput 2001; 13: 751-763.

[48] Houghton C, Kreuz T. On the efficient calculation of van Rossum distances. Network-Comp Neural 2012; 23: 48-58.

[49] Hindmarsh JL, Rose R. A model of neuronal bursting using three coupled first order differential equations. P R Soc B 1984; 221: 87-102.

[50] Crawford JD. Introduction to bifurcation theory. Rev Mod Phys 1991; 63: 991-1037.